



Article

Fast Synthesis of Au Nanoparticles on Metal–Phenolic Network for Sweat SERS Analysis

Xiaoying Zhang¹, Xin Wang², Mengling Ning³, Peng Wang², Wen Wang², Xiaozhou Zhang⁴, Zhiming Liu^{3,*} , Yanjiao Zhang^{4,*} and Shaoxin Li^{5,*}

¹ Department of Physical Education, Guangdong Medical University, Dongguan 523808, China

² School of Medical Technology, Guangdong Medical University, Dongguan 523808, China

³ Guangzhou Key Laboratory of Spectral Analysis and Functional Probes, College of Biophotonics, South China Normal University, Guangzhou 510631, China

⁴ School of Basic Medicine, Guangdong Medical University, Dongguan 523808, China

⁵ School of Biomedical Engineering, Guangdong Medical University, Dongguan 523808, China

* Correspondence: liuzm021@126.com (Z.L.); yjzhang@gdmu.edu.cn (Y.Z.); lishaox@163.com (S.L.)

Abstract: The biochemical composition of sweat is closely related to the human physiological state, which provides a favorable window for the monitoring of human health status, especially for the athlete. Herein, an ultra-simple strategy based on the surface-enhanced Raman scattering (SERS) technique for sweat analysis is established. Metal–phenolic network (MPN), an outstanding organic-inorganic hybrid material, is adopted as the reductant and platform for the in situ formation of Au-MPN, which displays excellent SERS activity with the limit of detection to 10^{-15} M for 4-mercaptobenzoic acid (4-MBA). As an ultrasensitive SERS sensor, Au-MPN is capable of discriminating the molecular fingerprints of sweat components acquired from a volunteer after exercise, such as urea, uric acid, lactic acid, and amino acid. For pH sensing, Au-MPN/4-MBA efficiently presents the pH values of the volunteer's sweat, which can indicate the electrolyte metabolism during exercise. This MPN-based SERS sensing strategy unlocks a new route for the real-time physiological monitoring of human health.

Keywords: surface-enhanced Raman scattering; metal–phenolic network; sweat; molecular fingerprint; pH



Citation: Zhang, X.; Wang, X.; Ning, M.; Wang, P.; Wang, W.; Zhang, X.; Liu, Z.; Zhang, Y.; Li, S. Fast Synthesis of Au Nanoparticles on Metal–Phenolic Network for Sweat SERS Analysis. *Nanomaterials* **2022**, *12*, 2977. <https://doi.org/10.3390/nano12172977>

Academic Editors:

Maurizio Muniz-Miranda and Onofrio M. Maragò

Received: 11 July 2022

Accepted: 26 August 2022

Published: 28 August 2022

Publisher's Note: MDPI stays neutral with regard to jurisdictional claims in published maps and institutional affiliations.



Copyright: © 2022 by the authors. Licensee MDPI, Basel, Switzerland. This article is an open access article distributed under the terms and conditions of the Creative Commons Attribution (CC BY) license (<https://creativecommons.org/licenses/by/4.0/>).

1. Introduction

Sweat is closely related to the physiological state of the human body, and its composition and pH value reflect different health conditions of the human body. Sweating has not only the function of regulating body temperature but also is an important excretory pathway to maintain a normal metabolism [1,2]. Sweat often contains a variety of electrolytes and metabolites, such as urea, uric acid, and lactic acid, as well as toxic substances after medication [3,4]. In view of the accessibility of sweat, the effective monitoring of sweat components is expected to be a simple and real-time means to assess human health status [5–7]. Exercise can accelerate the discharge of sweat, accompanied by a large number of metabolites, neurotransmitters, and other chemical molecules [8,9]. Ions such as Na^+ , Cl^- , and K^+ can also be flown out with perspiration, thereby affecting the pH value of sweat [10,11]. Excessive exercise may lead to excessive loss of mineral components in the body, causing electrolyte imbalance and endangering health [12]. The use of real-time portable photoelectric sensors helps to provide athletes with scientific sports data, formulate better training programs, and avoid training risk [13]. However, the accurate detection of a tiny volume of sweat is still a challenge [14].

The performance of photoelectric sensors largely depends on the properties of materials. Metal–phenolic network (MPN), an outstanding organic-inorganic hybrid material firstly reported by Caruso's group [15], has been widely used as a versatile coating material for multiple applications [16–20]. Different from other supramolecular structures,

the construction cost of MPN is low, and its synthesis is extremely simple that can be assembled on a large scale within 20 s [21]. For photoelectric sensing applications, MPN can be used as an excellent adhesive material for loading fluorescent molecules to realize multicolor fluorescent labeling and biosensor [22]. MPN can also serve as the soft metal probe for ultrasensitive electrochemical immunoassay [23]. In addition, MPN exhibits excellent reducing capacity allowing the fast generation of metal nanoparticles (NPs) on arbitrary material, which displays enhanced photoelectric features for photocatalysis and anti-microorganism [24–26]. Owing to the high affinity of MPN to biomolecules, the visualization and spectroscopic analysis of latent fingerprints have been realized by the formation of metal NPs on MPN [27]. This strategy is recently adopted for the fabrication of a three-dimensional surface-enhanced Raman scattering (SERS) sensor by in situ reductions of Ag NPs on MPN-coated commercial nanoanodic aluminum oxide film, achieving an ultrasensitive detection of raticide [28]. SERS has been proved to be a powerful analytical tool capable of providing the molecular fingerprint of the target [29]. SERS provides availability for the identification of biochemical components of a tiny sample with single-molecule accuracy [30,31]. SERS monitoring of the biochemical components in sweat samples is appealing, which can supply indicators of human health [32–34]. SERS-active nanostructures are also combined with flexible materials to fabricate wearable SERS sensors for real-time sweat monitoring [35–37]. Noble metal NPs such as Au, Ag, and Cu are commonly used as the active substrates for SERS analysis due to the Raman electromagnetic enhancement caused by the localized surface plasmon resonance (LSPR) effect. However, the SERS activities of discrete metal NPs are limited by their sparse “hot spots”.

Herein, a simple strategy for the SERS sensor is proposed by in situ rapid generations of Au NPs on MPN (Scheme 1). The as-prepared Au-MPN displays a film-like structure with densely scattered Au NPs, which generates abundant “hot spots”, achieving excellent SERS activity with the limit of detection (LOD) to 10^{-15} M for 4-mercaptobenzoic acid (4-MBA). The general surface binding affinity of MPN shows the great convenience of the nanocomposites to fabricate versatile SERS platforms. Au-MPN is then used as an ultrasensitive SERS substrate for the detection of the biochemical components of sweat samples acquired from a volunteer after exercise. In addition, a pH nanoprobe based on Au-MPN is established to monitor the electrolyte metabolism of the volunteer.



Scheme 1. Illustration of the MPN-based SERS substrate and its application for sweat sensing.

2. Materials and Methods

2.1. Reagents

Tannic acid (TA), chloroauric acid (HAuCl₄·4H₂O), and polyvinylpyrrolidone (PVP, K30) were purchased from China National Medicine Corporation (Shanghai, China). 3-(N-morpholino)propanesulfonic acid (MOPS) was obtained from Aladdin Reagent Co. Ltd. (Shanghai, China). Simulated sweat (pH 4.7, containing NaCl, urea, fatty acid, lactic acid, etc.) was purchased from Nanjing Xinfan Co. LTD, China. FeCl₃·6H₂O, 4-MBA, and other reagents were used as analytically pure grade. Deionized water (Milli-Q System, Millipore, Billerica, MA, USA) was used throughout the experiments.

2.2. Synthesis of MPN

PVP (1.5 mg/mL) and $\text{FeCl}_3 \cdot 6\text{H}_2\text{O}$ (0.12 mg/mL) were added to a flask containing deionized water (10 mL). Then TA (0.4 mg/mL) was added into the mixture and stirred for 20 min at room temperature. The as-prepared MPN was collected by centrifugation ($3000 \times g$, 10 min), and resuspended in deionized water.

2.3. Preparation of Au-MPN

HAuCl_4 (0.4 mM) was added into the eppendorf tubes containing 0.1 mg/mL MPN solution and quickly placed on a vortex mixer for 2 min. After standing for 10 min, the mixture was centrifuged at 3000 rpm for 10 min to collect Au-MPN. For the preparation of Au-MPNs with different Au/MPN ratios, HAuCl_4 with different concentrations (0.1, 0.2, 0.3, 0.4 and 0.5 mM) were used, named Au-MPN-1, Au-MPN-2, Au-MPN-3, Au-MPN-4 and Au-MPN-5, respectively.

2.4. Preparation of pH SERS Probe

4-MBA (10^{-4} M) was added into the eppendorf tubes containing Au-MPNs with various Au/MPN ratios and quickly placed on a vortex mixer for 2 min. After standing for 10 min, the mixture was centrifuged at 3000 rpm for 10 min to collect the pH-responsive SERS nanoprobe (Au-MPN/4-MBA).

2.5. Characterization

Transmission electron microscopy (TEM) was performed using a JEM-2100HR transmission electron microscope (JEOL, Tokyo, Japan) operated at 200 kV. Ultraviolet-visible (UV-VIS) absorbance spectra were acquired using a UV-VIS spectrometer (UV-6100, MAPADA, Shanghai, China). Raman spectra were recorded using a confocal microspectrometer (InVia, Renishaw, Derbyshire, England) equipped with a 785 nm laser. Fourier transform infrared (FT-IR) spectra were taken using a Nicoletti S50 spectrometer (Thermo, Waltham, MA, USA).

2.6. SERS Experiments

In order to optimize the Au/MPN ratio, Au-MPNs after grafting of 4-MBA were diluted into 0.2 mM and placed under the Renishaw Raman microscope for detection. A $20 \times$ objective lens was used to focus the laser beam and to collect the Raman signal. The Raman spectrum was acquired at a center wavelength of 1200 cm^{-1} under the 785 nm laser irradiation (5 mW, 6 s accumulation time). All the samples were measured at least five times.

Then, the optimal Au-MPN was mixed with different concentrations of 4-MBA (10^{-4} – 10^{-15} M) and detected under the Raman spectrometer to study the LOD of Au-MPN. For SERS repeatability analysis, the pH SERS probe was dropped onto an Al wafer to dry, and the SERS spectra at random 40 spots were collected. The intensity of the Raman band at 1078 cm^{-1} was used to calculate the relative standard deviation (RSD) value. For SERS image, the Raman mapping was performed in the streamline mode at wavenumber center 1200 cm^{-1} with 1 s of laser exposure (785 nm, 10 mW). The lateral resolution was $28 \mu\text{m}$, and a total of 3658 spectral lines were collected.

2.7. SERS Fingerprint Analysis of Sweat

Eleven volunteers (8 men, 3 women) with an age range of between 22–36 were recruited, and the volunteers gave written consent to participate in the study, which was approved by the Ethics Committee of Guangdong Medical University. After exercise, the sweat samples of the volunteers were collected for further analysis. Then $1 \mu\text{L}$ of sweat was dropped onto the pre-deposited Au-MPN substrate for SERS detection (785 nm laser, 10 mW, 6 s exposure time).

2.8. SERS pH Detection of Sweat

MOPS buffer solutions with the pH value from 3 to 10 were first prepared to assess the pH response characteristics of Au-MPN/4-MBA. One μL of pH sensor (2 mM) was mixed with 10 μL MOPS buffer, and the SERS spectrum was acquired. The pH-related SERS bands were selected to plot the pH response curve. After that, the simulated sweats with different pH values were used to record the pH-responsive dynamics of Au-MPN/4-MBA in order to get rid of the interference of other components in sweat. The pH value of real sweat collected from volunteer was determined using Au-MPN/4-MBA as the pH sensor according to the same SERS protocol. All the SERS detection was repeated at least five times.

3. Results and Discussion

3.1. Characterization of the Nanostructures

The formation of MPN film commonly involves a process of solid-phase template growth and etching [15]. Recently, Chen et al. proposed a strategy for controllable self-polymerization of MPN in the liquid phase by using polymer molecules [16]. Here we used PVP as the liquid-phase template to support the self-assembly of MPN. The morphology of MPN detected by TEM is shown in Figure 1A, where a film-like and porous structure is observed. Figure 1B displays the microstructure of MPN after in situ reductions of Au NPs, in which spherical Au NPs with a mean size of 52 nm are randomly dispersed on MPN film. The high-resolution TEM (HRTEM) image of Au-MPN reveals the amorphous structure of MPN and a crystalline structure of Au NP with a lattice spacing of about 0.24 nm (Figure 1C). The UV-VIS absorbance spectrum of MPN illustrates a typical absorption band at around 570 nm, which is consistent with that reported previously [16]. After Au NPs generation, a strong LSPR peak at 540 nm emerges (Figure 1D), and the synthetic efficiency of Au-MPN is ideal (Figure S1). The Raman spectra of MPN and Au-MPN (Figure 1E) show the characteristic Raman bands at 1350 and 1480 cm^{-1} , ascribing to the skeletal vibrations of the benzene ring [20]. In addition, the chemical composition of Au-MPN shows the common features of its precursors, as confirmed by the FT-IR spectra (Figure 1F), such as 1645 cm^{-1} (C=O stretching), 1440 cm^{-1} (C–O stretching), 1282 cm^{-1} (C–N stretching), 1192 cm^{-1} (O–H bending), and 1060 cm^{-1} (C–OH stretching) [26,38,39]. We also observe a reduced intensity of the C–OH band in the spectral lines of MPN and Au-MPN compared with that of TA, indicating the coordination of the phenolic groups with Fe ions [21].

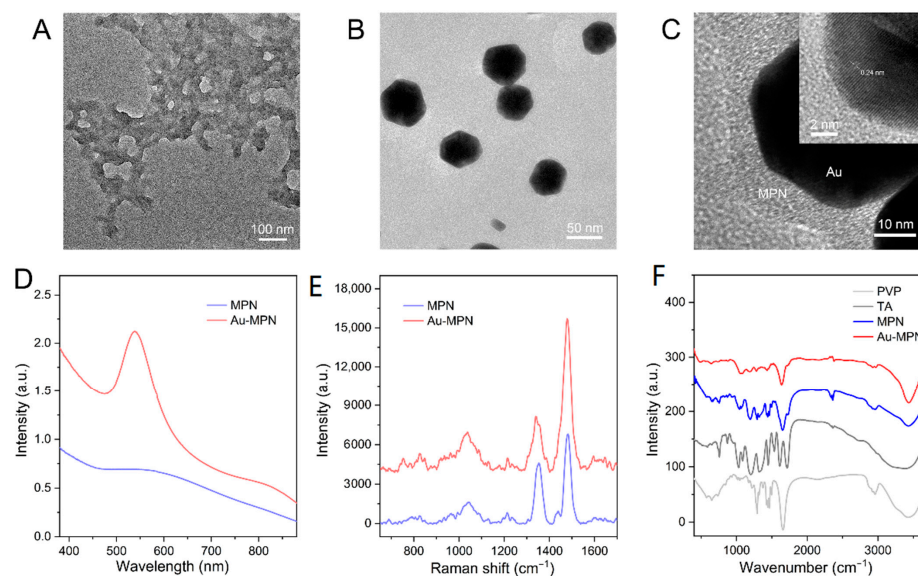


Figure 1. TEM images of MPN (A) and Au-MPN (B), respectively. (C) HRTEM image of Au-MPN (Insert shows the crystalline structure of Au NP). The UV-VIS absorbance (D), Raman (E) and the FT-IR (F) spectra of the nanostructures, respectively.

3.2. SERS Activities of Au-MPN

In order to investigate the optimal SERS activity, five Au-MPNs with different Au/MPN ratios were prepared. A red shift of the LSPR peak is observed in the UV-VIS absorbance spectra of Au-MPNs (Figure 2A), indicating an increasing size of Au NPs on MPN (Figure S2). Then 4-MBA molecules were grafted onto Au-MPNs (Figure S3). Figure 2B displays the SERS spectra of 4-MBA induced by those Au-MPNs, where Au-MPN-4 triggers the strongest SERS signals that can well match with the fingerprints of 4-MBA (Figure S4), and Au-MPN-4 was used for further experiments.

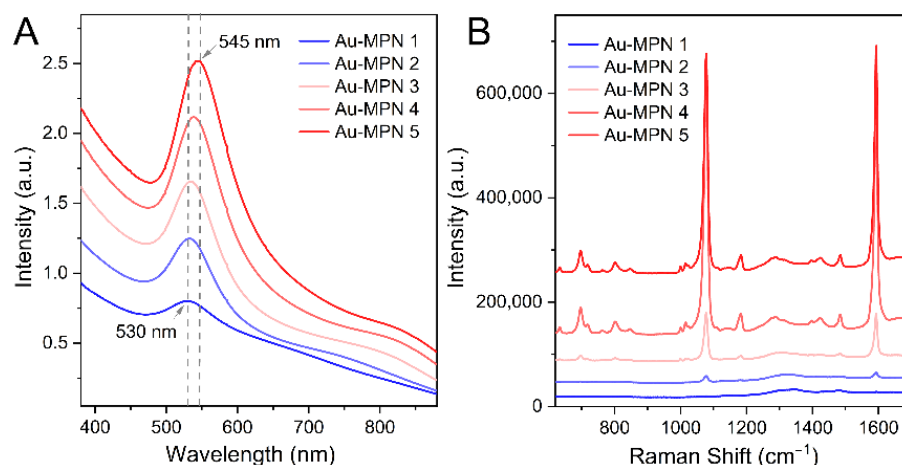


Figure 2. (A) UV-VIS absorbance spectra of Au-MPNs with different Au/MPN ratios and (B) their corresponding SERS activities to 4-MBA.

Then, different concentrations of 4-MBA molecules were deposited onto Au-MPN-4 for SERS detection. As shown in Figure 3A, the concentration-dependent SERS signals are observed at the concentration range of 4-MBA from 10^{-15} to 10^{-4} M. The SERS spectral pattern retains well though some peaks disappear at low 4-MBA concentrations. The major bands at 1078 and 1596 cm^{-1} assigned to the ring-breathing modes always exist, even if the concentration of 4-MBA decreases down to 10^{-15} M. To estimate the SERS repeatability, more than 40 SERS spectral lines of 4-MBA after grafting onto Au-MPN were collected (Figure 3C); and the SERS intensity of the Raman band at 1078 cm^{-1} was shown in Figure 3B, in which the RSD value was calculated to be 2.1%, indicating a good SERS reproducibility. We also plotted a SERS map of Au-MPN/4-MBA after drying, further confirming the SERS' good uniformity (Figure 3D).

3.3. Molecular Fingerprint of Human Sweat Induced by Au-MPN

The excellent SERS performance of Au-MPN endows it with great potential for the molecular fingerprint analysis of analytes with low scattering cross sections, such as biological samples. We recruited 11 volunteers (8 men, 3 women) and collected their sweats after exercise. The SERS spectra of these sweat samples were then acquired using Au-MPN as the ultrasensitive optical sensor. Figure 4A illustrates the molecular fingerprints of sweats of these 11 volunteers, where abundant fingerprint information is observed, such as 651 , 736 , 830 , 856 , 927 , 1003 , 1045 , 1080 , 1249 , 1322 , 1358 , 1457 , 1493 , 1589 , 1621 and 1648 cm^{-1} , etc. The biochemical assignments of these Raman bands are listed in Table 1. It can be clearly noticed that many vibrational modes are assigned to the major components of sweat (urea, uric acid, lactic acid, and amino acid) [40–44], indicating the potent potential of the Au-MPN-based SERS technique for sweat identification. The SERS spectra of volunteer sweats share a basic spectral pattern; however, the obvious difference is still noticed among these 11 spectral lines. For example, most SERS spectra exhibit a strong Raman peak at 1003 cm^{-1} , while the intensity of this band decreases dramatically in 5#, 9#, and 11#, revealing a low urea excretion in these three volunteers. In addition, a sharp SERS peak

at 1033 cm^{-1} that can be ascribed to uric acid [41,44] is observed in the spectral line of 9#, which may be an indicator of some physiological changes.

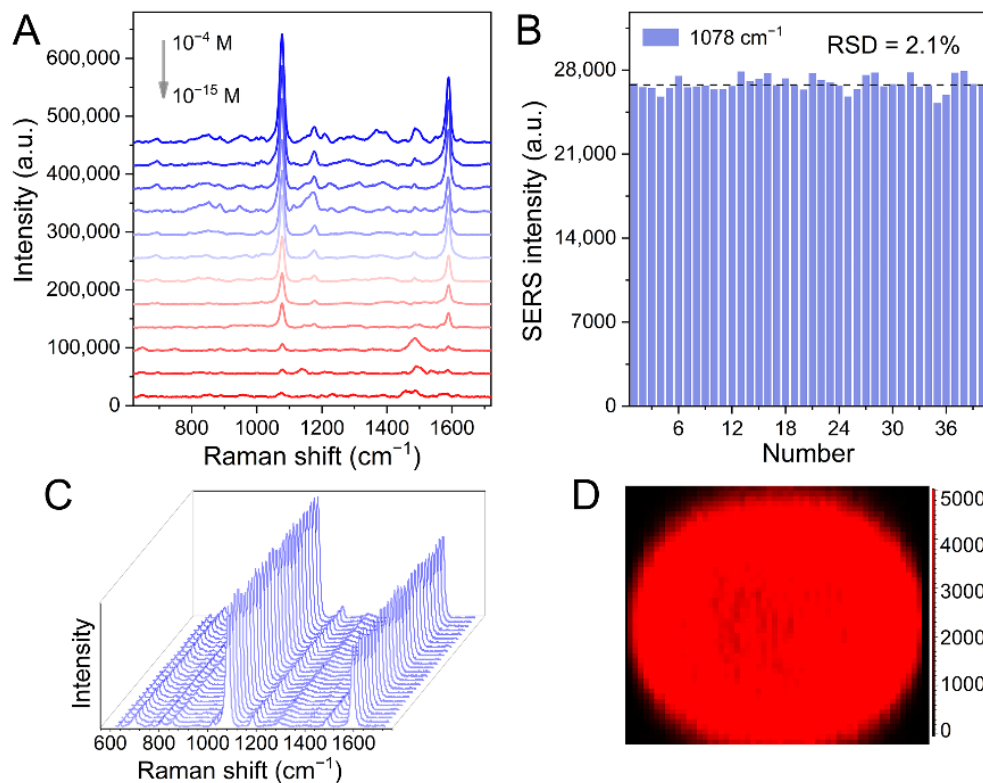


Figure 3. (A) SERS spectra of 4-MBA molecules at different concentrations deposited onto Au-MPN (Au-MPN-4). (B) SERS intensities of 1078 cm^{-1} peak acquired from random 40 SERS spectra (C) of 4-MBA grafted on Au-MPN. (D) SERS image of Au-MPN/4-MBA.

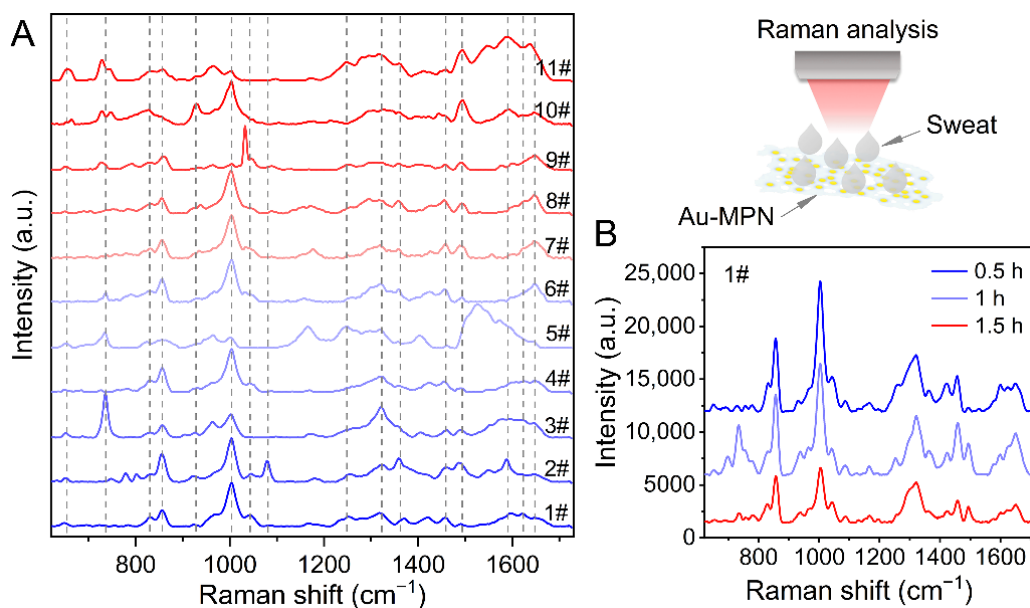


Figure 4. (A) SERS spectra of sweat samples collected from eleven volunteers (1#–8#, men; 9#–11#, women) using Au-MPN as the ultrasensitive optical sensor. (B) Time-resolved SERS spectra of sweat for volunteer 1# after exercise.

Table 1. Tentative assignments of the SERS bands of sweat induced by Au-MPN.

SERS Band/cm ⁻¹	Assignment (Vibrational Mode)	Origin
651	O=C–N– bending	amino acid
736	N–H bending	uric acid
830	$\rho(\text{CH}_3)$	amino acid, lactic acid
856	$\rho(\text{CH}_3)$	amino acid, lactic acid
927	$\nu(\text{C–CO}_2^-)$, $\nu(\text{C–CH}_3)$, $\delta(\text{CO}_2^-)$, $\rho(\text{CH}_3)$	amino acid, lactic acid
1003	$\nu(\text{C–N})$, aromatic ring vibration	urea, amino acid
1045	$\nu(\text{C–C})$	protein
1080	$\nu(\text{C–O})$, $\delta(\text{C–COH})$	lactic acid
1249	$\delta(\text{CH})$, amide III	protein
1322	$\delta(\text{CH})$, amide III	protein
1358	$\nu(\text{C–O})$	uric acid
1457	$\delta(\text{CH}_3)$	lactic acid
1493	$\nu(\text{C–N})$, $\nu(\text{C–C})$	uric acid
1589	$\nu(\text{C–N})$, $\nu(\text{CO}_2^-)$	uric acid, lactic acid
1621	$\nu_4(\text{NH}_2)$	urea
1648	$\nu_2(\text{NH}_2)$	urea

We also monitored the sweat composition change during exercise using the Au-MPN-based SERS technique. Figure 4B shows the SERS spectra of sweat samples collected from volunteer 1# at an interval of 30 min after exercise. It can be observed that the integrated SERS intensities of sweat decrease gradually with the extension of exercise time, indicating the content of biochemical components in sweat reduces after long-term exercise. Moreover, we can also notice the fluctuation of fingerprint information in the SERS spectra, such as 736, 830, 927, 1045, 1457, 1493, and 1648 cm⁻¹. Therefore, the Au-MPN-based SERS technique offers a simple and reliable sensing method for monitoring the physiological state of the human body.

3.4. pH Sensing Based on Au-MPN

The electrolyte content determines the pH value of sweat. 4-MBA is a well-defined pH-responsive molecule that has been widely used for pH sensing [14,45,46]. We also fabricated a pH SERS nanoprobe by covalently grafting 4-MBA onto Au-MPN. The thiol group of the 4-MBA molecule shows a strong affinity for Au NPs and forms a stable Au–S bond [47]. Thus, the Raman fingerprints of sulfur-contained molecules are more prone to be enhanced by the metal-based SERS substrates [48]. The SERS performance of Au-MPN/4-MBA in MOPS buffer solutions at different pH values is displayed in Figure 5A. It can be noticed that the SERS signals in three regions, 665–745 cm⁻¹ (Figure 5B), 775–880 cm⁻¹ (Figure 5D), and 1340–1460 cm⁻¹ (Figure 5F), change significantly related to pH. For quantitative analysis, the intensity ratios of 722 to 698 cm⁻¹, 845 to 805 cm⁻¹, and 1400 to 1596 cm⁻¹ as a function of pH were plotted, as shown in Figure 5C,E,G, respectively. The R² values of the fitting curves of I₇₂₂/I₆₉₈, I₈₄₅/I₈₀₅, and I₁₄₀₀/I₁₅₉₆ are calculated to be 0.998, 0.994, and 0.989, respectively, indicating the exponential relationship between the SERS signals with pH.

Then, we used simulated sweat to evaluate the availability of Au-MPN-based pH sensors in the status close to a real environment. The SERS spectra (Figure 6A) and enlarged spectral lines in the ranges of 665–745 (Figure 6B), 775–880 (Figure 6D), and 1340–1460 cm⁻¹ (Figure 6F) at various pH values exhibit similar trends in comparison with that in MOPS buffer. The fitting curves of I₇₂₂/I₆₉₈ (Figure 6C), I₈₄₅/I₈₀₅ (Figure 6E), and I₁₄₀₀/I₁₅₉₆ (Figure 6G) are also plotted, and the corresponding R² values are calculated to be 0.999, 0.989, and 0.988, respectively. Among that, I₇₂₂/I₆₉₈ may be the best indicator for the pH of sweat. It can be concluded that Au-MPN/4-MBA displays promising potential as an efficient SERS nanoprobe for pH sensing of real sweat samples.

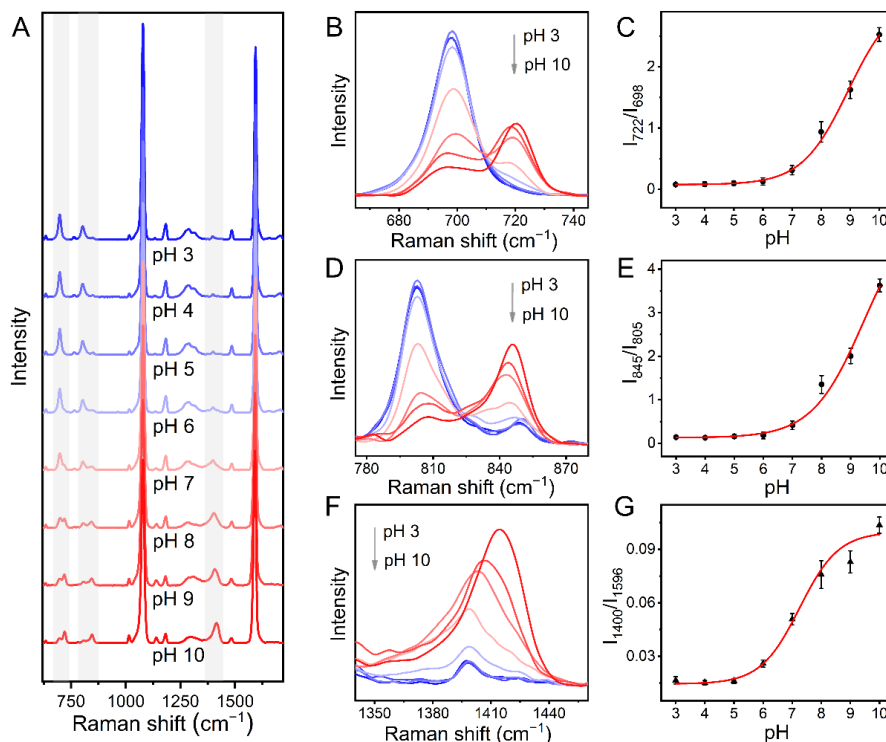


Figure 5. SERS spectra of Au-MPN/4-MBA in MOPS buffer solutions (A) with different pH values. Enlarged SERS spectra at the wavenumber ranges of 665–745 cm^{-1} (B), 775–880 cm^{-1} (D) and 1340–1460 cm^{-1} (F), respectively. SERS intensity ratios of 722/698 (C), 845/805 (E) and 1400/1596 (G) at different pH values, respectively.

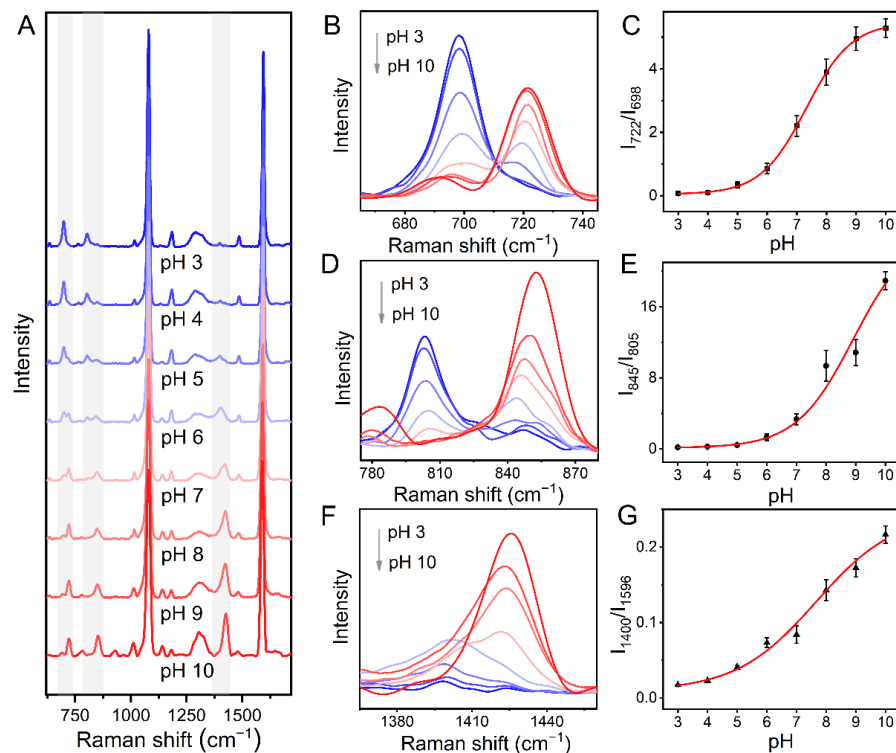


Figure 6. SERS spectra of Au-MPN/4-MBA in simulated sweats (A) with different pH values. Enlarged SERS spectra at the wavenumber ranges of 665–745 cm^{-1} (B), 775–880 cm^{-1} (D) and 1340–1460 cm^{-1} (F), respectively. SERS intensity ratios of 722/698 (C), 845/805 (E) and 1400/1596 (G) as a function of pH, respectively.

3.5. pH Monitoring of Human Sweat after Exercise

We finally utilized Au-MPN/4-MBA as novel pH SERS sensor for the detection of human sweat collected from a volunteer after exercise. The SERS spectra of 4-MBA in the sweat samples of the 11 volunteers are displayed in Figure 7A, where the Raman signals in the range of 665–745 cm^{-1} reflect the sweat pH. The pH values of the sweat samples were then calculated according to the fitting curve in Figure 6C. As demonstrated in Figure 7B, the pH values are situated in the range of 4.0–5.3 for the 11 volunteers. It can also be observed that the pH values of sweats for women are obviously higher than that for men. However, more sample data are needed to support this result. In addition, we monitored the change in pH value of sweat during exercise using Au-MPN/4-MBA. Figure 7C exhibits the SERS spectra and corresponding pH values of sweat samples acquired from volunteer 1# after exercise. We can notice that the pH value of sweat increases slightly during 1.5 h of perspiration, which may reflect the electrolyte metabolism level during exercise.

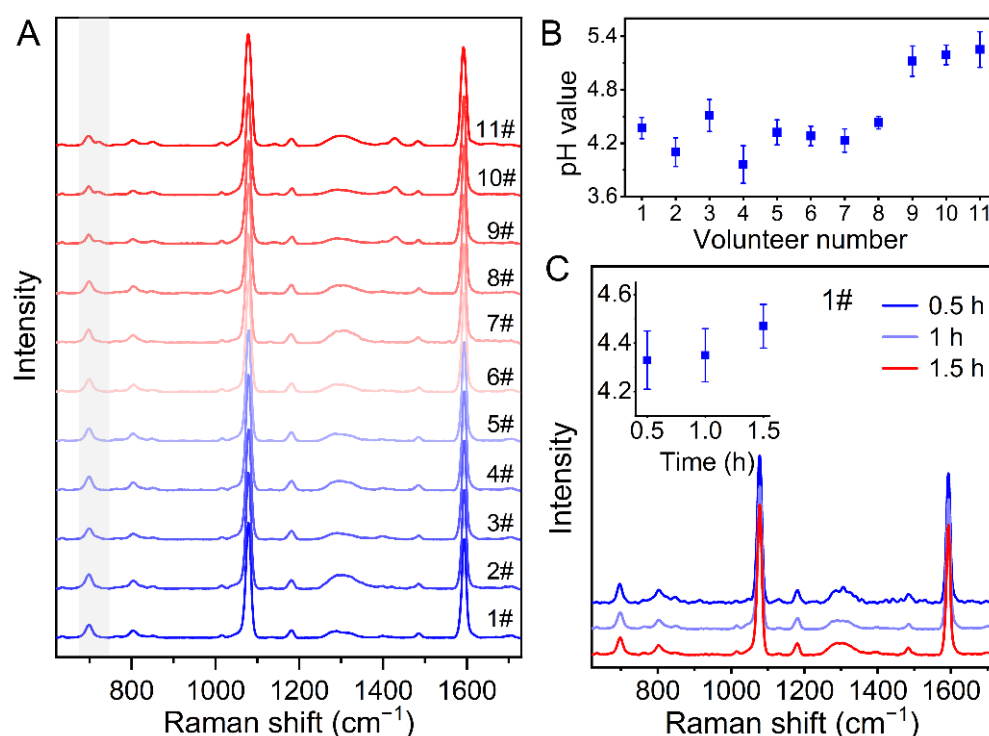


Figure 7. (A) SERS spectra of Au-MPN/4-MBA in the sweat samples acquired from eleven volunteers (1#–8#, men; 9#–11#, women). (B) The pH values of the sweat samples according to the values of I_{722}/I_{698} . (C) Time-resolved SERS-pH spectra of sweat and corresponding pH values for volunteer 1# after exercise.

4. Conclusions

In conclusion, an ultra-simple strategy for fabrication of SERS substrate is proposed by in situ reductions of AuNPs on supramolecular metal–organic networks. The versatile binding affinity of MPN endows Au-MPN with excellent SERS activity and repeatability for molecular detection, which exhibits a LOD value of 10^{-15} M for 4-MBA. For sweat fingerprint analysis, the Au-MPN-based SERS technique can efficiently distinguish the biochemical composition of sweat, such as urea, uric acid, lactic acid, and amino acid, which offers a reliable sensing method for the monitoring of physiological state during exercise. Au-MPN is also used to construct a pH SERS sensor by covalently grafting a pH-responsive 4-MBA molecule. The exponential relationship between the Raman signals with the pH values of sweat is observed in SERS spectra of Au-MPN/4-MBA. Using it as a novel pH SERS nanosensor, the pH values of the sweat samples acquired from volunteers are calculated to be 4.0–5.3, reflecting the electrolyte metabolism level during exercise.

This MPN-based SERS sensing strategy paves a new way for the real-time monitoring of exercise physiology.

Supplementary Materials: The following supporting information can be downloaded at: <https://www.mdpi.com/article/10.3390/nano12172977/s1>, Figure S1: UV-VIS spectra of Au-MPN before and after preparation; Figure S2: TEM images of Au-MPN-1, Au-MPN-2 and Au-MPN-4, respectively; Figure S3: UV-VIS spectra of Au-MPN before and after 4-MBA grafting; Figure S4: Normal Raman spectrum of 4-MBA (100 mM).

Author Contributions: Conceptualization, X.Z. (Xiaoying Zhang), Z.L., Y.Z. and S.L.; methodology, X.Z. (Xiaozhou Zhang) and Z.L.; software, X.W.; validation, M.N., P.W., W.W. and X.Z. (Xiaozhou Zhang); formal analysis, Y.Z.; investigation, X.Z. (Xiaoying Zhang), X.W. and M.N.; resources, S.L.; data curation, S.L.; writing—original draft preparation, X.Z. (Xiaoying Zhang) and Z.L.; writing—review and editing, X.W., M.N., P.W., W.W. and X.Z. (Xiaozhou Zhang); visualization, X.Z. (Xiaozhou Zhang); supervision, Z.L., Y.Z. and S.L.; project administration, Z.L.; funding acquisition, S.L. All authors have read and agreed to the published version of the manuscript.

Funding: Natural Science Foundation of Guangdong Province (No. 2019A1515012105, 2021A1515011733).

Institutional Review Board Statement: The study was conducted in accordance with the Ethics Committee of Guangdong Medical University.

Informed Consent Statement: Informed consent was obtained from all subjects involved in the study. Written informed consent has been obtained from the volunteers to publish this paper.

Data Availability Statement: Not applicable.

Acknowledgments: This work is supported by the Natural Science Foundation of Guangdong Province (No. 2019A1515012105, 2021A1515011733).

Conflicts of Interest: The authors declare no conflict of interest.

References

1. Chen, Y.-L.; Kuan, W.-H.; Liu, C.-L. Comparative Study of the Composition of Sweat from Eccrine and Apocrine Sweat Glands During Exercise and in Heat. *Int. J. Environ. Res. Public Health* **2020**, *17*, 3377. [[CrossRef](#)] [[PubMed](#)]
2. Bourque, C.W. Central Mechanisms of Osmosensation and Systemic Osmoregulation. *Nat. Rev. Neurosci.* **2008**, *9*, 519–531. [[CrossRef](#)] [[PubMed](#)]
3. Saat, M.; Sirisinghe, R.G.; Singh, R.; Tochiyama, Y. Effects of Short-Term Exercise in the Heat on Thermoregulation, Blood Parameters, Sweat Secretion and Sweat Composition of Tropic-Dwelling Subjects. *J. Physiol. Anthropol. Appl. Hum. Sci.* **2005**, *24*, 541–549. [[CrossRef](#)] [[PubMed](#)]
4. Morgan, R.M.; Patterson, M.J.; Nimmo, M.A. Acute Effects of Dehydration on Sweat Composition in Men during Prolonged Exercise in the Heat. *Acta Psychiatr. Scand.* **2004**, *182*, 37–43. [[CrossRef](#)]
5. Jiang, D.; Xu, C.; Zhang, Q.; Ye, Y.; Cai, Y.; Li, K.; Li, Y.; Huang, X.; Wang, Y. In-Situ Preparation of Lactate-Sensing Membrane for the Noninvasive and Wearable Analysis of Sweat. *Biosens. Bioelectron.* **2022**, *210*, 114303. [[CrossRef](#)]
6. Steijlen, A.S.M.; Jansen, K.M.B.; Bastemeijer, J.; French, P.J.; Bossche, A. Low-Cost Wearable Fluidic Sweat Collection Patch for Continuous Analyte Monitoring and Offline Analysis. *Anal. Chem.* **2022**, *94*, 6893–6901. [[CrossRef](#)]
7. Liao, J.; Zhang, X.; Sun, Z.; Chen, H.; Fu, J.; Si, H.; Ge, C.; Lin, S. Laser-Induced Graphene-Based Wearable Epidermal Ion-Selective Sensors for Noninvasive Multiplexed Sweat Analysis. *Biosensors* **2022**, *12*, 397. [[CrossRef](#)]
8. Nunes, M.J.; Cordas, C.M.; Moura, J.J.G.; Noronha, J.P.; Branco, L.C. Screening of Potential Stress Biomarkers in Sweat Associated with Sports Training. *Sports Med. Open* **2021**, *7*, 8. [[CrossRef](#)]
9. Harshman, S.W.; Browder, A.B.; Davidson, C.N.; Pitsch, R.L.; Strayer, K.E.; Schaeublin, N.M.; Phelps, M.S.; O'Connor, M.L.; Mackowski, N.S.; Barrett, K.N.; et al. The Impact of Nutritional Supplementation on Sweat Metabolomic Content: A Proof-of-Concept Study. *Front. Chem.* **2021**, *9*, 659583. [[CrossRef](#)]
10. Patterson, M.J.; Galloway, S.D.R.; Nimmo, M.A. Effect of Induced Metabolic Alkalosis on Sweat Composition in Men. *Acta Psychiatr. Scand.* **2002**, *174*, 41–46. [[CrossRef](#)]
11. Patterson, M.J.; Galloway, S.D.R.; Nimmo, M.A. Variations in Regional Sweat Composition in Normal Human Males. *Exp. Physiol.* **2000**, *85*, 869–875. [[CrossRef](#)] [[PubMed](#)]
12. Bennet, D.; Khorsandian, Y.; Pelusi, J.; Mirabella, A.; Pirrotte, P.; Zenhausern, F. Molecular and Physical Technologies for Monitoring Fluid and Electrolyte Imbalance: A Focus on Cancer Population. *Clin. Trans. Med.* **2021**, *11*, e461. [[CrossRef](#)] [[PubMed](#)]
13. Su, B.; Li, J.; Xu, H.; Xu, Z.; Meng, J.; Chen, X.; Li, F. Scientific Athletics Training: Flexible Sensors and Wearable Devices for Kineses Monitoring Applications. *Sci. Sin. Inform.* **2022**, *52*, 54–74. [[CrossRef](#)]

14. Chung, M.; Skinner, W.H.; Robert, C.; Campbell, C.J.; Rossi, R.M.; Koutsos, V.; Radacsi, N. Fabrication of a Wearable Flexible Sweat pH Sensor Based on SERS-Active Au/TPU Electrospun Nanofibers. *ACS Appl. Mater. Interfaces* **2021**, *13*, 51504–51518. [[CrossRef](#)] [[PubMed](#)]
15. Ejima, H.; Richardson, J.J.; Liang, K.; Best, J.P.; van Koeveden, M.P.; Such, G.K.; Cui, J.; Caruso, F. One-Step Assembly of Coordination Complexes for Versatile Film and Particle Engineering. *Science* **2013**, *341*, 154–157. [[CrossRef](#)]
16. Chen, J.; Pan, S.; Zhou, J.; Lin, Z.; Qu, Y.; Glab, A.; Han, Y.; Richardson, J.J.; Caruso, F. Assembly of Bioactive Nanoparticles via Metal–Phenolic Complexation. *Adv. Mater.* **2022**, *34*, 2108624. [[CrossRef](#)]
17. Zhang, Z.; Xie, L.; Ju, Y.; Dai, Y. Recent Advances in Metal–Phenolic Networks for Cancer Theranostics. *Small* **2021**, *17*, 2100314. [[CrossRef](#)]
18. Xie, L.; Li, J.; Wang, G.; Sang, W.; Xu, M.; Li, W.; Yan, J.; Li, B.; Zhang, Z.; Zhao, Q.; et al. Phototheranostic Metal–Phenolic Networks with Antiexosomal PD-L1 Enhanced Ferroptosis for Synergistic Immunotherapy. *J. Am. Chem. Soc.* **2022**, *144*, 787–797. [[CrossRef](#)]
19. Xu, C.; Peng, C.; Yang, X.; Zhang, R.; Zhao, Z.; Yan, B.; Zhang, J.; Gong, J.; He, X.; Kwok, R.T.K.; et al. One-Pot Synthesis of Customized Metal–Phenolic-Network-Coated Aie Dots for in Vivo Bioimaging. *Adv. Sci.* **2022**, *9*, 2104997. [[CrossRef](#)]
20. Zhou, M.; Zhao, C.; Li, Y.; Guo, Y.; Liu, H.; Zhang, Y.; Liu, Z. Facile Synthesis of Metal-Phenolic-Coated Gold Nanocuboids for Surface-Enhanced Raman Scattering. *Appl. Opt.* **2020**, *59*, 6124–6130. [[CrossRef](#)]
21. Guo, J.; Ping, Y.; Ejima, H.; Alt, K.; Meissner, M.; Richardson, J.J.; Yan, Y.; Peter, K.; von Elverfeldt, D.; Hagemeyer, C.E.; et al. Engineering Multifunctional Capsules through the Assembly of Metal–Phenolic Networks. *Angew. Chem. Int. Ed.* **2014**, *53*, 5546–5551. [[CrossRef](#)] [[PubMed](#)]
22. Lin, Z.; Zhou, J.; Qu, Y.; Pan, S.; Han, Y.; Lafleur, R.P.M.; Chen, J.; Cortez-Jugo, C.; Richardson, J.J.; Caruso, F. Luminescent Metal-Phenolic Networks for Multicolor Particle Labeling. *Angew. Chem. Int. Ed.* **2021**, *60*, 24968–24975. [[CrossRef](#)] [[PubMed](#)]
23. Huang, J.; Meng, J.; Chen, S.; Zhang, S.; Liu, T.; Li, C.; Wang, F. A Soft Metal-Polyphenol Capsule-Based Ultrasensitive Immunoassay for Electrochemical Detection of Epstein-Barr (EB) Virus Infection. *Biosens. Bioelectron.* **2020**, *164*, 112310. [[CrossRef](#)] [[PubMed](#)]
24. Yun, G.; Besford, Q.A.; Johnston, S.T.; Richardson, J.J.; Pan, S.; Biviano, M.; Caruso, F. Self-Assembly of Nano- to Macroscopic Metal–Phenolic Materials. *Chem. Mater.* **2018**, *30*, 5750–5758. [[CrossRef](#)]
25. Yun, G.; Pan, S.; Wang, T.-Y.; Guo, J.; Richardson, J.J.; Caruso, F. Synthesis of Metal Nanoparticles in Metal-Phenolic Networks: Catalytic and Antimicrobial Applications of Coated Textiles. *Adv. Healthc. Mater.* **2018**, *7*, 1700934. [[CrossRef](#)] [[PubMed](#)]
26. Guo, Z.; Lu, J.; Xie, W.; Li, X.; Wu, H.; Zhao, L. Facile Preparation of Recyclable Fe@Metal Phenolic Networks-Au System for Catalytic Reduction of 4-Nitrophenol. *Mater. Chem. Phys.* **2022**, *281*, 125907. [[CrossRef](#)]
27. Yun, G.; Richardson, J.J.; Capelli, M.; Hu, Y.; Besford, Q.A.; Weiss, A.C.G.; Lee, H.; Choi, I.S.; Gibson, B.C.; Reineck, P.; et al. The Biomolecular Corona in 2D and Reverse: Patterning Metal–Phenolic Networks on Proteins, Lipids, Nucleic Acids, Polysaccharides, and Fingerprints. *Adv. Funct. Mater.* **2020**, *30*, 1905805. [[CrossRef](#)]
28. Sun, J.; Xue, D.; Shan, W.; Liu, R.; Liu, R.; Zhao, H.; Li, T.; Wang, Z.; Zhang, J.; Shao, B. In Situ Growth Large Area Silver Nanostructure on Metal Phenolic Network Coated Nano Film and Its SERS Sensing Application for Monofluoroacetic Acid. *ACS Sens.* **2021**, *6*, 2129–2135. [[CrossRef](#)]
29. Wang, X.; Huang, S.-C.; Hu, S.; Yan, S.; Ren, B. Fundamental Understanding and Applications of Plasmon-Enhanced Raman Spectroscopy. *Nat. Rev. Phys.* **2020**, *2*, 253–271. [[CrossRef](#)]
30. Choi, H.K.; Lee, K.S.; Shin, H.H.; Koo, J.J.; Yeon, G.J.; Kim, Z.H. Single-Molecule Surface-Enhanced Raman Scattering as a Probe of Single-Molecule Surface Reactions: Promises and Current Challenges. *Acc. Chem. Res.* **2019**, *52*, 3008–3017. [[CrossRef](#)]
31. Langer, J.; Jimenez de Aberasturi, D.; Aizpurua, J.; Alvarez-Puebla, R.A.; Auguie, B.; Baumberg, J.J.; Bazan, G.C.; Bell, S.E.J.; Boisen, A.; Brolo, A.G.; et al. Present and Future of Surface-Enhanced Raman Scattering. *ACS Nano* **2020**, *14*, 28–117. [[CrossRef](#)] [[PubMed](#)]
32. Cai, R.; Yin, L.; Huang, Q.; You, R.; Feng, S.; Lu, Y. An Endoscope-Like SERS Probe Based on the Focusing Effect of Silica Nanospheres for Tyrosine and Urea Detection in Sweat. *Nanomaterials* **2022**, *12*, 421. [[CrossRef](#)] [[PubMed](#)]
33. Kim, H.S.; Kim, H.J.; Lee, J.; Lee, T.; Yun, J.; Lee, G.; Hong, Y. Hand-Held Raman Spectrometer-Based Dual Detection of Creatinine and Cortisol in Human Sweat Using Silver Nanoflakes. *Anal. Chem.* **2021**, *93*, 14996–15004. [[CrossRef](#)] [[PubMed](#)]
34. Ma, H.; Cui, Q.; Xu, L.; Tian, Y.; Jiao, A.; Wang, C.; Zhang, M.; Li, S.; Chen, M. Silk Fibroin Fibers Decorated with Urchin-Like Au/Ag Nanoalloys: A Flexible Hygroscopic SERS Sensor for Monitoring of Folic Acid in Human Sweat. *Opt. Express* **2021**, *29*, 30892–30904. [[CrossRef](#)] [[PubMed](#)]
35. Wang, Y.; Zhao, C.; Wang, J.; Luo, X.; Xie, L.; Zhan, S.; Kim, J.; Wang, X.; Liu, X.; Ying, Y. Wearable Plasmonic-Metasurface Sensor for Noninvasive and Universal Molecular Fingerprint Detection on Biointerfaces. *Sci. Adv.* **2021**, *7*, eabe4553. [[CrossRef](#)]
36. Mogera, U.; Guo, H.; Namkoong, M.; Rahman, M.S.; Nguyen, T.; Tian, L. Wearable Plasmonic Paper-Based Microfluidics for Continuous Sweat Analysis. *Sci. Adv.* **2022**, *8*, eabn1736. [[CrossRef](#)]
37. Koh, E.H.; Lee, W.-C.; Choi, Y.-J.; Moon, J.-I.; Jang, J.; Park, S.-G.; Choo, J.; Kim, D.-H.; Jung, H.S. A Wearable Surface-Enhanced Raman Scattering Sensor for Label-Free Molecular Detection. *ACS Appl. Mater. Interfaces* **2021**, *13*, 3024–3032. [[CrossRef](#)]
38. Saroj, A.L.; Singh, R.K.; Chandra, S. Studies on Polymer Electrolyte Poly(Vinyl) Pyrrolidone (PVP) Complexed with Ionic Liquid: Effect of Complexation on Thermal Stability, Conductivity and Relaxation Behaviour. *Mater. Sci. Eng. B* **2013**, *178*, 231–238. [[CrossRef](#)]

39. Xu, W.; Pan, S.; Noble, B.B.; Chen, J.; Lin, Z.; Han, Y.; Zhou, J.; Richardson, J.J.; Yarovsky, I.; Caruso, F. Site-Selective Coordination Assembly of Dynamic Metal-Phenolic Networks. *Angew. Chem. Int. Ed.* **2022**, *61*, e202208037. [[CrossRef](#)]
40. Sikirzhytski, V.; Sikirzhytskaya, A.; Lednev, I.K. Multidimensional Raman Spectroscopic Signature of Sweat and Its Potential Application to Forensic Body Fluid Identification. *Anal. Chim. Acta* **2012**, *718*, 78–83. [[CrossRef](#)]
41. Westley, C.; Xu, Y.; Thilaganathan, B.; Carnell, A.J.; Turner, N.J.; Goodacre, R. Absolute Quantification of Uric Acid in Human Urine Using Surface Enhanced Raman Scattering with the Standard Addition Method. *Anal. Chem.* **2017**, *89*, 2472–2477. [[CrossRef](#)] [[PubMed](#)]
42. Olaetxea, I.; Valero, A.; Lopez, E.; Lafuente, H.; Izeta, A.; Jaunarena, I.; Seifert, A. Machine Learning-Assisted Raman Spectroscopy for pH and Lactate Sensing in Body Fluids. *Anal. Chem.* **2020**, *92*, 13888–13895. [[CrossRef](#)] [[PubMed](#)]
43. Verma, M.; Naqvi, T.K.; Tripathi, S.K.; Kulkarni, M.M.; Prasad, N.E.; Dwivedi, P.K. Plasmonic Paper-Based Flexible SERS Biosensor for Highly Sensitive Detection of Lactic and Uric Acid. *IEEE Trans. Nanobiosci.* **2022**, *21*, 294–300. [[CrossRef](#)]
44. Li, Y.; Chen, H.; Guo, Y.; Wang, K.; Zhang, Y.; Lan, P.; Guo, J.; Zhang, W.; Zhong, H.; Guo, Z.; et al. Lamellar Hafnium Ditetelluride as an Ultrasensitive Surface-Enhanced Raman Scattering Platform for Label-Free Detection of Uric Acid. *Photon. Res.* **2021**, *9*, 1039–1047. [[CrossRef](#)]
45. Pallaoro, A.; Braun, G.B.; Reich, N.O.; Moskovits, M. Mapping Local pH in Live Cells Using Encapsulated Fluorescent SERS Nanotags. *Small* **2010**, *6*, 618–622. [[CrossRef](#)] [[PubMed](#)]
46. Talley, C.E.; Jusinski, L.; Hollars, C.W.; Lane, S.M.; Huser, T. Intracellular pH Sensors Based on Surface-Enhanced Raman Scattering. *Anal. Chem.* **2004**, *76*, 7064–7068. [[CrossRef](#)] [[PubMed](#)]
47. Aina, V.; Marchis, T.; Laurenti, E.; Diana, E.; Lusvardi, G.; Malavasi, G.; Menabue, L.; Cerrato, G.; Morterra, C. Functionalization of Sol Gel Bioactive Glasses Carrying Au Nanoparticles: Selective Au Affinity for Amino and Thiol Ligand Groups. *Langmuir* **2010**, *26*, 18600–18605. [[CrossRef](#)]
48. Schwartz-Duval, A.S.; Konopka, C.J.; Moitra, P.; Daza, E.A.; Srivastava, I.; Johnson, E.V.; Kampert, T.L.; Fayn, S.; Haran, A.; Dobrucki, L.W.; et al. Intratumoral Generation of Photothermal Gold Nanoparticles through a Vectorized Biomineralization of Ionic Gold. *Nat. Commun.* **2020**, *11*, 4530. [[CrossRef](#)]